

Novel Liposomal Drug Delivery of Tecomaquinone I for Oral Squamous Cell Carcinoma as a Potential Therapeutic Strategy- An Invitro Study

Mudiyayirakkani Muthusamy^{1*}, Pratibha Ramani¹, Bargavi¹, Ramya Ramadoss²,
Raghunandhakumar³, Balachander Kannan⁴

¹Department of Oral and Maxillofacial Pathology, Saveetha Dental College and Hospitals, Saveetha institute of Medical and technical sciences, Vellapanchavadi, Chennai, 600077, Tamil Nadu, India

²Department of Oral Biology, Saveetha Dental College and Hospitals, Saveetha Institute of Medical and Technical Sciences, Vellapanchavadi, Chennai, 600077, Tamil Nadu, India

³Cancer and Stem cell research Lab, Department of Pharmacology, Saveetha Dental College and Hospitals, Saveetha Institute of Medical and technical sciences, Vellapanchavadi, Chennai, 600077, Tamil Nadu, India

⁴Molecular Biology Laboratory, Centre for cellular and Molecular research, Saveetha Dental College and Hospitals, Saveetha Institute of Medical and Technical Sciences, Vellapanchavadi, Chennai, 600077, Tamil Nadu, India

Abstract

Oral cancer is one of the most common cancers in the world and 90% of the oral cancers are oral squamous cell carcinoma (OSCC). The treatment modalities of oral squamous cell carcinoma includes surgery, chemotherapy and radiotherapy. Though these treatment modalities are considered to be effective, they have their own adverse effects. Treating OSCC with a plant-based drug through an effective drug delivery system may increase the quality of life of the patients. The aim of this study is to formulate a liposomal drug delivery of Tecomaquinone I for oral squamous cell carcinoma. Tecomaquinone I extract of *Tectona grandis* Linn was extracted. Pegalated liposome infused with Tecomaquinone I extract was fabricated using conventional method. The MDA-MB-231, A549 and SCC-25 cancer cell lines were treated with the pegalated liposome infused with Tecomaquinone I to analyse the cell cycle arrest, cytotoxic effects and apoptotic effects of Tecomaquinone I. Liposomal Tecomaquinone I showed substantial accumulation of cells in the G2/M phase, indicative of mitotic arrest and enhanced apoptotic cell death in SCC-25 (OSCC) cell line. Tecomaquinone I exerts potent cell cycle arrest, cytotoxic and apoptotic effects on Oral squamous cell carcinoma cell line (SCC-25).

Keywords: Farnesyl Transferase Inhibitor, Liposomal Drug Delivery, Oral Squamous Cell Carcinoma, Phytocompound, Tecomaquinone I.

Introduction

Drug delivery is a method of administering a pharmaceutical compound inside the body to achieve a therapeutic effect. The mode of drug delivery plays important role in proper delivery of the drug to its site of interest, concentration of the drug and in degradation of the drug. A mode of drug delivery is considered preminent

if the drug delivery is slow, targeted and controlled. One such mode of drug delivery is liposomal drug delivery [1].

Liposomes are novel drug delivery system. They are microscopic vesicular structures which is made up of lipid bilayer. Their advantage is that they exhibit a tailored drug release according to the need of the body at the

particular time and also directs the place of action increasing the therapeutic index of the drug. They are vesicles composed of lipids, fatty acid, drug molecules. It differs in size, composition, particle charge according to the materials used in formulating the liposome [2]. They play vital role in the purview of targeted therapy. They are used in the medical field for treating various diseases like lung diseases, ocular disorders, vaccine adjuvant, infectious diseases, cancer therapy, brain disorders. The novel drug delivery system of liposomes can also be used in the treatment of oral cancer [3-8].

Cancer is the leading cause of death worldwide. Among all the cancers, oral cancer ranks 11th worldwide [9]. India has the most number of oral cancer cases accounting for men (11.28% of all cancers) and it is the fifth most common in women (4.3% of all cancers). Oral squamous cell carcinoma (OSCC) is the most common form of oral malignancy accounting for 80-90% of the cases [10]. OSCC being a multifactorial disease, it is caused by tobacco, alcohol, microbial factors, genetic predisposition, sharp tooth, diet, family history, immune deficiency [11-13].

The development of oral squamous cell carcinoma in the purview of genetic alteration is a multistep process which may be due to

overexpression or inactivation of the oncogenes or the tumor suppressor genes by mutations, loss of heterozygosity, deletions or epigenetic modifications such as methylation [14]. The oncogenes and the tumor suppressor genes wheel up the process of carcinogenesis by increasing the number of tumor cells by stimulation of formation of new cells or by inhibiting the cell death or cell cycle arrest. The increase in number of cells can be caused by the activation of the genes that drive the cell cycle, by inhibiting normal apoptotic processes or by facilitating the provision of nutrients through enhanced angiogenesis [15]. RAS is an oncogene that encodes cell membrane associated proteins which are involved in the transduction of extracellular growth, differentiation and survival signal [16]. The HRAS, KRAS and NRAS gene belongs to the RAS oncogene family. The HRAS gene provides the signal for producing the HRAS protein which is responsible for regulating the cell division in response to the stimulation of growth factors. HRAS acts as a molecular button as once it is turned on it results in activation of proteins that results in signal transduction leading to cell growth, division and proliferation (Figure 1). These events are the effects of the process known as prenylation [17].

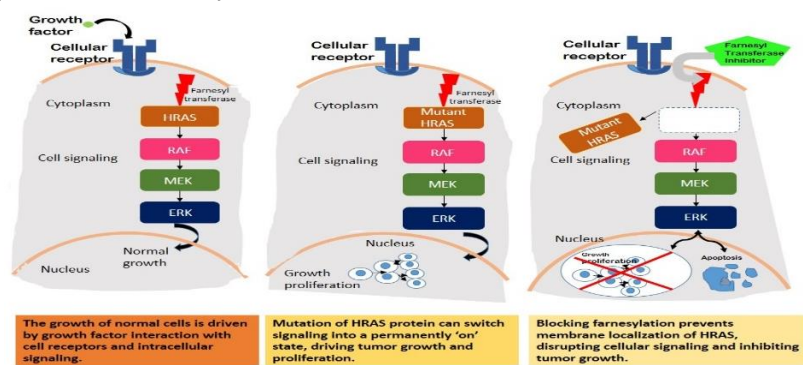


Figure 1. The RAS Pathway and the Role of Farnesyl Transferase and Farnesyl Transferase Inhibitor in RAS Pathway

Prenylation is the post-translational modifications that are required for the transforming activity of many oncogenic proteins including RAS facilitating the

attachment of the proteins to the cell membrane. Prenylation is a combination of two entities namely farnesylation and genarylgenarylation [18, 19].

Farnesylation is the addition of farnesyl group to the proteins in the presence of the enzyme farnesyl transferase. This farnesylation helps in the maturation of RAS into active form. This highlights that inhibition of the farnesyl transferase would block farnesylation of RAS, reverse RAS mediated cellular transformations, induce apoptosis and regulates cell cycle [20]. The use of farnesyl transferase inhibitor will play a vital role in the treatment of oral squamous cell carcinoma.

The treatment modalities for oral squamous cell carcinoma are surgical resection of the tumour, radiotherapy and chemotherapy [21]. Though these treatments are gold standard they also have adverse effects like oral mucositis, xerostomia, osteoradionecrosis, tissue fibrosis that highly affects the quality of life of the treated patients. The chemotherapeutic drugs used in the treatment of oral squamous cell carcinoma causes severe tiredness, alopecia, infections, anemia, bruising and bleeding and loss of appetite. In order to overcome this pathetic episode, chemical formulations can be replaced with phytochemical formulations.

Medicinal plants are the rich sources of ingredients known as phytochemicals which plays a significant role in drug development, treating and preventing disease conditions. According to the WHO, approximately 21,000 species of plants have the ability to be used as medicine. The main reason for using medicinal plants is due to their better cultural acceptability, better compatibility and adaptability with the human body and exhibit lesser adverse effects [22]. Because of their wide chemical makeup and a varied array of biological activities, phytochemicals have become an inevitable part in the field of medicine. The various bioactive compounds found in plants are flavonoids, terpenoids, polyphenols, calchones, quinolones, quinones, sequitrenes, coumarins, alkaloids, tannins, amides, and several additional unidentified molecules with multifaceted pharmacological effects. These chemicals can interact with

cellular targets, making them potent chemotherapeutic agents [23]. The most favourable feature of phytochemicals is their selective cytotoxic effects on cancer cells through the targeting of particular pathways, which ultimately lead to the inhibition of the growing tumour cells and the induction of programmed cell death. Over time, this will reduce the damage that is caused to the healthy cells. Additionally, phytochemicals have potent anti-oxidant and anti-inflammatory characteristics that will reduce the inflammation and reactive oxygen species, which are known to be crucial in the initiation and advancement of cancer. Because of their reduced toxic profiles and higher tolerance, these phytochemicals will increase the quality of life of the chemotherapeutic patients, decrease treatment interruptions, and promote long-term adherence [24].

One such medicinal plant is *Tectona grandis*. Linn.f.(*Teak*). It has a tremendous amount of medicinal values which are still being unexplored. The plant has many biologically active components like quinones, lapachol, flavonoids, terpenes, lignans, sterols, apocarotenoids, sterols, fatty acids, steroids, alkanes that possess high antioxidant activity [25]. A particular active component known as Tecomaquinone I which is a naphthoquinone is a potent farnesyl transferase inhibitor [26]. When this active component Tecomaquinone I is extracted and formulated to a liposome, it will be a promising therapeutic strategy for oral squamous cell carcinoma. So, we conducted an insilico study and an extensive in vitro research to experiment the effect of the liposomal drug delivery of Tecomaquinone I in oral squamous cell carcinoma.

Materials and Methods

This research was approved by the scientific review board of the institution and the SRB reference number is **SRB/SDC/PhD/OPATH-2001/22/096**.

***In silico* Analysis**

Structure Retrieval

The structure of HRAS was retrieved from PDB (Id: 121P) (Figure 2a) and was refined and minimized by using Swiss- PdbViewer and the structure of Tecomaquinone I was retrieved from Pubchem database (Id: 3574508) (Figure 2b)

Pharmacophore Modelling and Virtual Screening

The pdb structure of HRAS has a co-crystallize compound which was used to generate the pharmacophore model using Molecular Operating Environment. The compound Tecomaquinone I was docked with the receptor HRAS.

Docking Dynamics

Desmond, a software from Schrödinger LLC was used to model molecular dynamics for 100 nanoseconds. The first step in molecular dynamics simulation of receptor and ligand complexes are docking experiments. In static situations, the ligand-binding states can be predicted by molecular docking studies. Docking plays a crucial role in exhibiting the static view of a molecule's binding pose at an RNA's active site. The integration of Newton's classical equation of motion simulates atom movements by time through molecular docking. Simulations were used to predict the ligand-binding status in physiological atmosphere.

Protein preparation Wizard of Maestro was used to preprocess the receptor–ligand complex, optimization and minimization. System Builder tool was used to prepare all the systems. TIP3P, a solvent model with an orthorhombic box, was chosen. (Transferable Intermolecular Interaction Potential 3 Points). The OPLS 2005 force field was used in the simulation. Counter ions were introduced to make the models neutral. 0.15 M sodium chloride (NaCl) was added in order to mimic physiological conditions. For the entire

simulation, the NPT ensemble with 300 K temperature and 1 atm pressure. Before the simulation the models were relaxed. After every 100 ps the trajectories were saved for examination and the comparison of root mean square deviation (RMSD) value of the protein and ligand was done to verify the simulation stability.

***In vitro* Analysis**

Isolation of Extract from *Tectona grandis* Linn

The root of *Tectona grandis* Linn was taken and minced by using mortar and pestle after which half of the quantity was treated with 5 ml of chloroform overnight and the other half of the quantity was treated with 5ml of white petroleum overnight. The chloroform extract and the white petroleum extract were collected separately and stored at 4°C for future use [27].

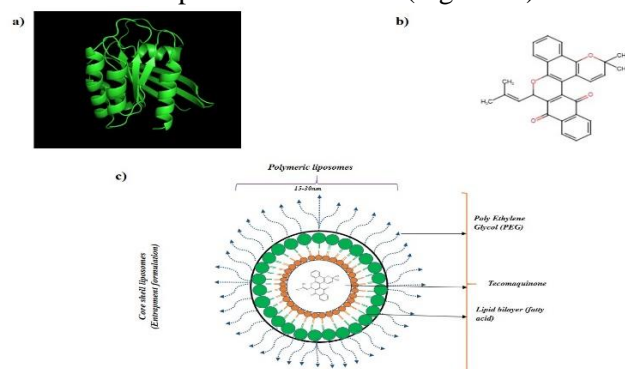
Incorporation of Silver Nanoparticle to The Extract

About 5 ml of chloroform extract was added with 50 ml of distilled water and around 80mg of silver nitrate (AgNO_3) in a beaker which was placed on the stirrer for 3 hours. Similarly, 5 ml of the white petroleum extract was added with 50 ml of distilled water and around 80mg of silver nitrate (AgNO_3) in a beaker which was placed on the stirrer for 3 hours. These silver nanoparticle extract form the active components containing the drug [28, 29].

Formulation of Liposome

The liposomes were synthesized using the conventional method. Initially, around 2ml of silver nanoparticle incorporated chloroform extract, 2 ml of silver nanoparticle incorporated white petroleum extract were added with 10ml of chloroform and 10ml of methanol in a beaker and subjected to continuous stirring for about 30 minutes. This was followed by addition of 2ml of omega 3 fatty acid after which it was left in heat overnight allowing it to evaporate. Then around 10 ml of polyethylene glycol (PEG) was

added and subjected to stirring for 3 hours [30, 31]. This process led to an end product of



Tecomaquinone I infused pegalated liposomes. (Figure 2c).

Figure 2. A) The PDB Structure of HRAS Gene, B) Shows the Structure of Tecomaquinone I C) Shows the Schematic Representation of the Manufactured Liposome with Tecomaquinone I

Characterization

The structural and morphological properties of the extract was examined using Scanning Electron Microscopy (SEM) (Jeol JSM-IT800 Nano SEM) and elemental analysis was done by using EDS (Oxford instruments). Functional groups and the bonding nature of the compounds were examined by Fourier-transform infrared spectroscopy (FT-IR) (Perkin Elmer). The absorbance spectra of the extract was measured by using the Ultraviolet-visible Spectroscopy (UV-vis) (JASCO).

The structural and morphological properties of the liposomes were examined using Transmission Electron Microscopy (HR-TEM) (FEI Tecnai G² 20 S-TWIN).

Scanning Electron Microscopy with Energy Dispersive X-ray Spectroscopy (SEM-EDS)

Scanning electron microscopy is used to produce images of the given sample by scanning the surface with a focused beam of electrons. The electrons will interact with the atoms in the sample resulting in production of signals that contain information about the surface topography and composition of the sample. The energy dispersive X-ray spectroscopy is an analytical technique which is used for the elemental analysis or chemical characterization of a sample. It relies on an interaction of some source of x-ray excitation

and a sample. The synthesized AgNPs were morphologically characterized using SEM and was analysed by placing the sample in the carbon stub in the scanning electron microscope at an accelerated voltage of 30kV.

Fourier-Transform Infrared Spectroscopy (FT-IR)

Fourier transform infrared spectroscopy is a technique used to obtain an infrared spectrum of absorption or emission of a solid, liquid or gas.

Ultraviolet-Visible Spectroscopy (UV-vis)

UV visible spectroscopy is used for the quantitative determination of diverse analytes. Analysing the UV absorbance spectra of extracts from teak (*Tectona grandis*) roots using petroleum jelly and chloroform involves several key steps. This method helps identify compounds within the extracts that absorb UV light, which can indicate the presence of bioactive molecules such as phenolics, flavonoids, or terpenoids. It is done by measuring the intensity of light that passes through the sample with respect to the intensity of light through a reference sample. It is done to measure the conjugation of silver (Ag) and the extract (Tecomaquinone I). The sample is loaded in the cuvette and analyzed in the wavelength of 440 nm.

High Resolution- Transmission Electron Microscopy (HR-TEM)

High resolution transmission electron microscopy is a technique in which provides the direct image of atomic structure of the samples. It makes use of the phase contrast imaging that combines both transmitted and scattered electrons to construct image. It helps in providing quantitative and qualitative, structural and chemical characterization at a nanoscale. The structural characterization of the liposome was assessed by using HRTEM (FEI Tecnai G² 20 S-TWIN) by initially drying the diluted liposome on a carbon coated TEM copper grids followed by measurement at an accelerated voltage of 200 kV with magnification of 25X-1030X, point resolution of 0.24nm and line resolution of 0.14nm.

Minimal Inhibitory Concentration of the Liposomes (Time Dependant Growth Inhibition Assay)

Minimal inhibitory concentration (MIC) is defined as the minimum concentration of the drug that is required to inhibit the growth of the particular organism. Growth curve was used to assess the bacterial growth. On Muller Hinton Agar (MHA) and 50 mL of Luria-Bertaini (LB) media, new colonies were injected. The reference for the growth limit was an optical density of 0.1 at 600 nm (O.D. of 0.1 equals to 108 CFU/mL of media). Additional samples were introduced on their own as well as 2 108 CFU/mL of control organisms such *Escherichia coli*, *Staphylococcus aureus*, *Candida albicans*, *Enterococcus faecalis*, and *Streptococcus mutans*. Every flask was incubated at 37 °C for 50 rpm while being shaken after which the tube was left undisturbed for 24 hours at 37°C.

Hemocompatibility of the Liposomes

The hemocompatibility of the liposomes were assessed by in vitro hemolysis (ASTM F756-08). 5ml of blood was collected from a healthy volunteer using a sterile syringe and

was transferred to an Ethylene Diamine Tetra Acetic acid (EDTA) tube to avoid coagulation. Then the mixture was centrifuged at 4000 rpm at 4°C for 10 minutes. The collected erythrocytes (RBCs) were further washed by using Phosphate Buffer Saline (PBS) of pH 7.4. Then the RBCs were mixed with suitable amount of Phosphate Buffer Saline (PBS) with the pH of 7.4 in a centrifuge tube. After this, around 10 µl of diluted liposomes (9 parts of PBS in 1 part of liposomes) were mixed with 1ml of RBCs in PBS (pH 7.4) and incubated at 37°C for 1 hour with mild shaking. There are two other tubes containing positive control and negative control. The positive control tube consists of 1ml of RBCs in water and the negative control tube consists of the 1ml of RBCs in PBS (pH 7.4). The hemolytic percentage was obtained by using the equation

$$\text{Hemolytic percentage} = \frac{\text{Sample absorbance} - \text{Negative Control}}{\text{Positive Control} - \text{Negative control}} \times 100$$

Drug Release

Drug release is the process in which drug solutes migrate from the initial position in the polymeric system to the polymer's outer surface and then to the release medium. There are several mechanisms through which the drug release is controlled in a system like dissolution, diffusion, osmosis, partitioning, swelling, erosion and targeting. This is done to assess the efficacy and quality of the drug delivery system. Around 1ml of the pegalated liposome loaded with Tecomaquinone I was taken in a dialysis membrane (with an appropriate molecular weight cutoff, typically 10–14 kDa) (Himedia) and was suspended in a beaker containing 50ml of Phosphate buffer saline at 37°C (release media, pH 7.4, or other physiologically relevant media) under continuous stirring mimicking physiological conditions. At predetermined time intervals (e.g., 0.5, 1, 2, 4, 6, 12, 24 hours), around 1ml of the aliquots (phosphate buffer saline) was taken and was replaced with 1ml of fresh phosphate buffer saline to maintain sink

conditions. The liposomes in the release medium were incubated and the aliquots were sampled at the predetermined intervals. The aliquots were centrifuged to separate the liposomes and the supernatant was analyzed for the released Tecomaquinone I. The concentration of Tecomaquinone Is measured from the collected samples using the calibration curve.

In Vitro

Experimental Group

Group 1: Control/ without induction, Group 2: Liposomal Tecomaquinone I (LP), Group 3: Tipifarnib (TF)

1. Cell Line Culture and Expansion

Prior to the in vitro cell culture study, The MDA-MB-231, A549 and SCC-25 cancer cell line was procured from NCCS, Pune India and ATCC - USA. The high glucose media containing Dulbecco's Modified Eagle Medium (DMEM), 10% Fetal Bovine Serum (FBS) V/V and 1% antibiotic/antimycotic penicillin and streptomycin (W/V) was used to sub-culture the cancer cells. The cancer cells were grown in CO₂ incubator with 5% carbon dioxide and 95% humidity as recommended by NCCS for this particular cell line.

2. Cytotoxicity Assay

The anti-proliferative activity of control and experimental group on MDA-MB-231, A549 and SCC-25 cells was determined over 24hr by MTT assay were studied by MTT assay. Briefly, after incubation with control and experimental group on MDA-MB-231, A549 and SCC-25 cells were seeded on 96 well culture plate for 24 hr respectively. To determine the percentage of cell viability, the post incubated cells were replaced with 10 μ l of stock MTT dye (10 mg/ml) was added in each well and plate was incubated again at 37 °C for 4 h. The medium was replaced with 100 μ l DMSO in each well to dissolve the formazan crystals and absorbance was recorded at 570 nm. with Synergy hybrid

Multi-Mode Reader (BioTek, Winooski, VT, US). The percent cell viability was calculated using the following equation:

$$\text{Cell viability (\%)} = \frac{OD(\text{test sample}) - OD(\text{Blank})}{OD(\text{PC}) - OD(\text{blank})} \times 100$$

3. Deal Staining of Acridine Orange-Ethidium Bromide (AO/EtBr)

The AO/EtBr dual staining procedure was used to monitor the death of tumour cells and apoptosis induction. MDA-MB-231, A549 and SCC-25 cells were seeded at a concentration of 1×10^5 mL⁻¹ per well into a 24-well microtiter plate and incubated overnight at 37 °C, 5% CO₂. After incubation, cells were treated with control and experimental group, and allowed the cells to incubate for another 24 h. After that, the cells were rinsed twice with PBS to remove the medium and an aliquot of 100 μ L of dual fluorescent dye (equal volume of AO and EtBr, 10 μ g mL⁻¹) was added to each well and then visualizing the cells under a fluorescence inverted microscope (Invitrogen, evos). Identification criteria were concentrated green areas of chromatin condensation in the nucleus considered early apoptosis, green intact nuclei considered viable cells and dense orange areas of chromatin condensation and intact nuclei considered late apoptosis.

4. ROS Determination by DCFH-DA Assay

The Reactive Oxygen Species was generated during apoptosis. The ROS generated was measured by Dichlorodihydro- fluorescein diacetate (DCFH-DA) staining method. The MDA-MB-231, A549 and SCC-25 cells treated for 24hrs with control and experimental group were subjected to DCFH-DA staining and incubated at dark condition for 30 min. The ROS generated in the cytoplasm was detected inverted Phase contrast fluorescence microscopy (Invitrogen, evos). Viable cells, exhibiting green fluorescence, were stained by DCFH-DA and detected using green filter.

5. Evaluation of DNA Fragmentation by DAPI Staining

Cell apoptosis of MDA-MB-231, A549 and SCC-25 cells induced by control and experimental group were determined by DAPI staining. Cells were seeded on 24-well with a density of 5×10^4 cells/well and treated with experimental group at low, medium, high concentrations for 24 h. Cells were fixed with 4% paraformaldehyde in PBS for 30 min at room temperature, followed by permeabilization with 0.25% Triton X-100 in PBS for 30 min and stained with DAPI for 4 min in dark. The unstained and stained cells were observed under Phase contrast inverted fluorescence microscopy (Invitrogen, evos).

6. Cell Cycle Distribution Analysis

Cells were plated into 6-cell plates at a density of 2×10^5 cells/well and treated with experimental group along with positive control and control group for 24hrs. Then, cells were fixed in ice-cold ethanol (70%) at 4 °C overnight and suspended in PBS containing 0.1% Triton X-100 and 100 µg/mL RNase A. After that, cells were incubated in 5 µL of PI solution for 30 min and analyzed by flow cytometer FACS canto II (BD Biosciences, San Jose, CA, USA). Data were analyzed using Flow Jo Software (BD Biosciences, San Jose, CA, USA).

Flow Cytometry

Flow cytometry is a qualitative technique used to measure the physical and chemical characteristic attributes of a population of cells. It also helps in the accurate analysis of cell cycle in either live or fixed cell populations. It estimates the percentage of cell population in different phases of cell cycle namely the G0, G1, S, G2, M phases respectively. The cells are stained with a fluorochrome dye. Analysis by flow cytometry is based on the fluorescence intensity of the nuclei stained with the fluorochrome. The flow cytometric analysis of the cell count versus the linear fluorescence is used to create histogram across the phases of

the cell cycle. Standard modelling algorithms are used to determine the breakdown of cells in the G0/G1 phase versus S phase, G2 or polyploidy state of the cell population.

Apoptosis Assay

Apoptosis assay was carried out using Annexin V and PI (BD Biosciences, USA). After 12 hours of culture with and without the compound, the cells were harvested and spun down. The supernatant was discarded and resuspended in a binding buffer. Then the cells were stained using Annexin V FITC (5 µl), Propidium Iodide (5 µl) for 15 minutes at room temperature. After incubation, 400 µl of 1X binding buffer was added to all the tubes and acquired using BD FACSLyric flow cytometer (BD Biosciences, USA). The analysis was performed using FACSuite 4.1 software.

Cell Cycle Analysis

Cells were spun down, supernatant discarded, washed thrice using buffer and resuspended in 250 µl of solution A (contains trypsin in a spermine tetrahydrochloride detergent for digestion of cell membrane) and incubated for 10 minutes at room temperature. Then 200 µl of solution B (containing trypsin inhibitor and ribonuclease A to digest RNA) was added on top of it and incubated for 10 minutes at room temperature. Then 200 µl of Solution C (containing PI that binds to DNA) was finally added on top of it and incubated at 4degree C for 10 minutes. Then the cells were acquired (10000 events) using BD FACSLyric flow cytometer. The analysis was performed using FAC Suite 4.1 software.

Results

Insilico Analysis

The merged pharmacophore model with matching features such as hydrogen bond donors, hydrogen bond acceptors, aromatic rings is shown in Figure 3a. The Root Mean Square Deviation (RMSD) is used to measure the average change in displacement of selection

of atoms for a particular frame with respect to a reference frame. The above figure shows the RMSD evolution of protein (left y-axis) and ligand (right y-axis), respectively. Monitoring the RMSD of protein can give the structural conformation throughout the simulation and the RMSD of ligand indicates the stability of the ligand with respect to the protein and its binding pocket. From the above plot (Figure 3b), it shows that the RMSD of the protein HRAS fluctuates within 2.4 Å upto 60 ns and the RMSD value of the ligand Tecomaquinone I fluctuates within 2 Å upto 60 ns. The fluctuations of the RMSD values of both protein and ligand fluctuates within 1.0 ns which is normal. Figure 3c shows most of the ligand protein interactions determined with the molecular dynamics are hydrophobic interactions. In term of hydrophobic interactions, ALA_18, ILE_21, PHE_28, VAL_29, TYR_32, PRO_34, LYS_117, ALA_146 are the most important for HRAS-Tecomaquinone I complex. The stacked bar charts are normalized over the course of the trajectory for example: a value of 0.8 suggests that 80% of the stimulation time the specific interaction is maintained. Sometimes, a value

more than 1 is also possible because some protein residue may make multiple contacts of same subtype with the ligand. The Residue Mean Square Fluctuation (RMSF) is useful for characterizing local changes along the protein chain. The above plot (Figure 3d) explains the RMSF for the residue. The peaks in the plot indicates the areas of proteins that fluctuates the most during the simulations. The low RMSF value indicates that the protein and ligand complex has higher stability to the binding site residues. Figure 3e represents the ligand protein contacts explaining the detailed ligand atom interactions with the protein residues. Generally, interactions that occur more than 30% of the simulation time in the selected trajectory are shown and around 71% of the interactions that happen seems to be hydrophobic. The protein secondary structure elements (SSE) like the alpha helices and the beta strands are monitored throughout the simulation. Figure 3f represents the distribution of the SSE by the residue index throughout the protein structure. Figure 3g represents the position of docked Tecomaquinone I with HRAS proteins.

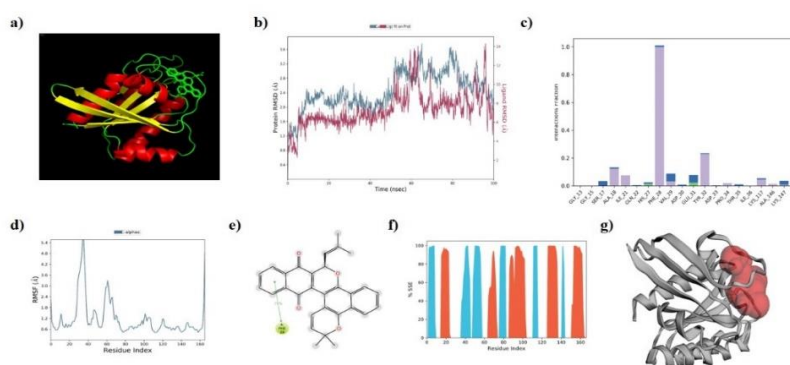


Figure 3. a) merged pharmacophore model of HRAS gene (protein) and Tecomaquinone I (ligand) with possible H-bond donor and acceptor groups b) Plot of Root Mean Square Deviation (RMSD) of HRAS and Tecomaquinone I as a function of time c) Evaluation of active sites and other binding site residues for HRAS protein and Tecomaquinone I d) RMSF calculation of Tecomaquinone I which indicates the protein area that fluctuates the most during the course of MD simulation e) The 2D representation of Tecomaquinone I and the residues involved in interaction with amino acid residues f) Protein secondary structure elements (SSE) (red-alpha helices, blue-beta strands) of M pro with the reports of SSE distribution by residue and the summary of the SSE composition of each trajectory frame over the course of simulation g) The binding pose of Tecomaquinone I and HRAS protein at the receptor binding domain of HRAS

Invitro Analysis

Scanning Electron Microscopy (SEM)

Tecomaquinone I-Chloroform Extract

The SEM and EDS analysis revealed and confirmed the presence of silver nanoparticles. The SEM images of the Tecomaquinone I-Chloroform extract revealed that the nanoparticles are spherical in shape and the size of the nanoparticles ranges from 40-80nm which is dispersed homogeneously (Figure 4a). The obtained nanoparticle was extracted at room temperature of 37°C. The SEM images of the Tecomaquinone I-white petroleum extract revealed that the nanoparticles are hexagonal in shape and the size of the nanoparticles ranges from 5nm to 300 nm which is dispersed homogeneously (Figure 4b). The obtained nanoparticle was extracted at room temperature of 37°C.

Energy Dispersive Spectroscopy (EDS)

Energy dispersive spectroscopy (EDS) is a tool to analyze the elemental composition of the material. The EDS of Tecomaquinone I-chloroform shows that the extract has 66.9% of silver (Ag) (Figure 4c) and the EDS of Tecomaquinone I- white petroleum shows that the extract has 94.7% of silver (Ag) it also has other elements like 8.9% of carbon (C), 3.9% of oxygen (O), 0.9% of chloride (Cl) (Figure 4d) which may be from the plant extract.

FT-IR

The FTIR analysis of Tecomaquinone I-chloroform extract showed the presence of normal polymeric OH stretch (3435.83 cm^{-1}) in the single bond region, Cyanide ion, thiocyanate ion, and related ions (2077.73 cm^{-1}) in the triple bond region, Alkenyl C=C stretch (1638.27 cm^{-1}) in the double bond region, Alkyne C-H bend, Aliphatic bromo compounds, C-Br stretch, Alcohol, OH out-of-plane bend (660.04 cm^{-1}) in the fingerprint region (Figure 4e). The FTIR analysis of Tecomaquinone I-white petroleum extract

showed the presence of Hydroxy group, H-bonded OH stretch (3445.13 cm^{-1}) in the single bond region, Transition metal carbonyls (2087.09 cm^{-1}) in the triple bond region, Alkenyl C=C stretch (1638.42 cm^{-1}) in the double bond region, Alkyne C-H bend, Aliphatic bromo compounds, C-Br stretch, Alcohol, OH out-of-plane bend (668.98 cm^{-1}) in the fingerprint region (Figure 4f).

UV

The visual spectrograph of the AgNPs have been recorded as a function of time. Absorption spectra of the AgNPs in the reaction media have absorbance peak between 430 nm and 440 nm for Tecomaquinone I- white petroleum AgNP and 450 nm for Tecomaquinone I- chloroform AgNP and the peaks tend to be broad showing that the particles are polydispersed (Figure 4g). For UV-Vis Spectroscopy, Dilute the extracts to an appropriate concentration using a suitable solvent (e.g., chloroform for chloroform extracts and a compatible solvent for petroleum jelly extracts). UV-Vis absorbance spectra of each extract in the range of 200–800 nm were recorded, which is typically used for UV analysis. UV spectra showing peaks around 250–290 nm and 320–360 nm could indicate the presence of Tecomaquinone I. Generally, 250–290 nm: Associated with $\pi \rightarrow \pi^*$ transitions in the aromatic or conjugated double-bond systems. And 320–360 nm: Related to $n \rightarrow \pi^*$ transitions in the carbonyl (C=O) group.

High resolution Transmission electron microscopy (HR-TEM)

The structural analysis was done for the liposomes carrying the AgNPs by using HR-TEM (FEI Tecnai G² 20 S-TWIN) which revealed that the size of liposomes to be < 20nm that are of spherical in shape and is bilamellar in nature with the coating of AgNP (drug), fatty acid (middle layer) and polyethylene glycol (outer layer) (Figure 4h).

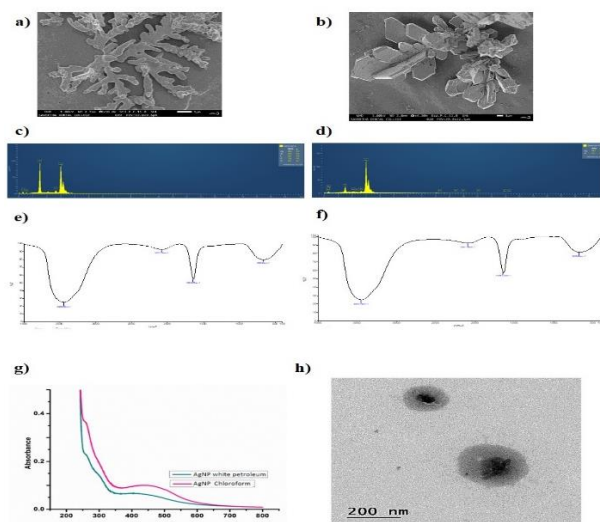


Figure 4. a) SEM image of Tecomaquinone I- Chloroform extract b) SEM image of Tecomaquinone I- white petroleum extract c) EDS image of Tecomaquinone I- chloroform extract d) EDS image of Tecomaquinone I- white petroleum extract e) FTIR of Tecomaquinone I- chloroform extract f) FTIR of Tecomaquinone I- white petroleum extract g) UV analysis of Tecomaquinone I- chloroform and Tecomaquinone I- white petroleum extract h) HRTEM image of the fabricated pegalated liposome

MIC

After 24 hours of incubation at 37°C, to evaluate the reduction in bacterial growth, optical density measurements for 24 h time points at 600 nm were made (Figure 5a). The pegalated liposome (PL) showed better inhibitory effects than the control and non-pegalated liposome (L). It shows that the pegalated liposome inhibited the growth of *E. faecalis*, *C. albicans*, *S. mutans* with an MIC value of 0.0 µg/ml, the growth of *S. aureus* with an MIC value of 0.01 µg/ml, the growth of *E. coli* with an MIC value of 0.09 µg/ml.

Hemocompatibility

The results are presented as percent hemolysis. On observing, our liposomes and the PEG- liposomes did not affect the RBCs. The hemolysis rates determined in the presence of the formulations did not exceed the negative control more than 0.4% of the negative control, which explains that the liposomes are non-

hemolytic according to the ASTM F756-08 standards (Figure 5b).

Drug Release

Initial burst release is due to surface-adsorbed. High encapsulation efficiency suggests that the liposomal formulation effectively incorporates Tecomaquinone I. A prolonged release pattern implies that the liposomes successfully deliver the drug over an extended period, reducing dosing frequency. Initial rapid drug release could indicate surface-adsorbed Tecomaquinone I. The analysis provides insights into how effectively liposomes serve as carriers for Tecomaquinone I. Parameters like high encapsulation efficiency, sustained release, stability, enhanced bioactivity, and reduced cytotoxicity underline the potential for liposomal formulations in drug delivery systems. Within 12 h around 56 % of drugs has been released (Figure 5c).

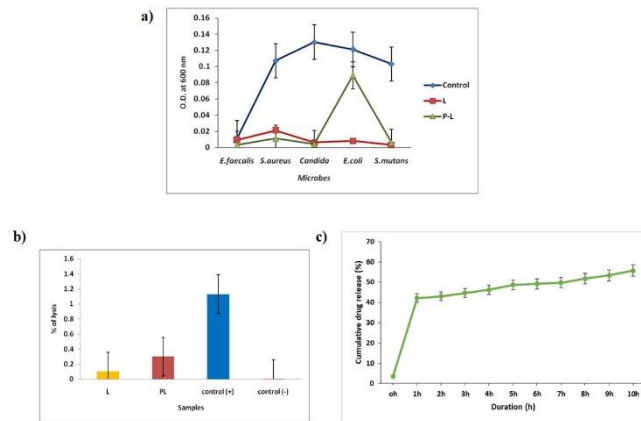


Figure 5. a) Minimal inhibitory concentration of the Tecomaquinone I extract b) Hemocompatibility of Tecomaquinone I extract c) Drug release of the Tecomaquinone I from the liposomal formulation.

MTT

Cell Viability Assay (MTT)

The cytotoxic effects of TF (Tipifarnib), LP (Tecomaquinone I) on MDA-MB-231, A549 and SCC-25 cells. Cells were treated with TF

and LP (0-50 $\mu\text{g/ml}$ concentration) for 24 h, and cell viability was evaluated by MTT assay. Data are shown as means \pm SD (n = 3). * Compared with the control blank group, $p < 0.001$ (Figure 6).

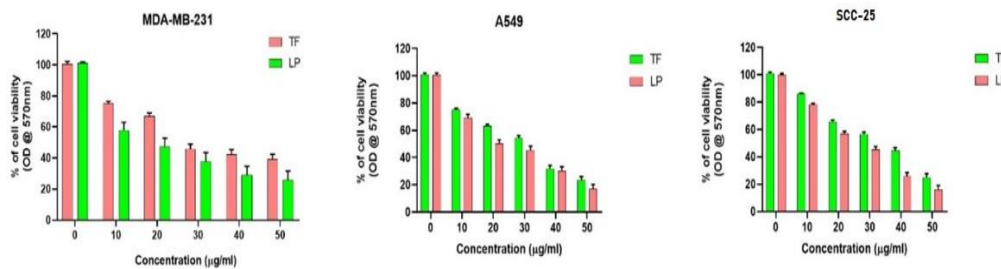


Figure 6. The Concentration ($\mu\text{g/ml}$) of Tipifarnib (TF) and Liposomal Tecomaquinone I (LP) and the % of Viable Cells (MDA-MB-231, A549, SSC-25)

TF and LP (20 and 30 $\mu\text{g/ml}$) on MDA-MB-231

Cells were treated with TF and LP (20 and 30 $\mu\text{g/ml}$) on MDA-MB-231 cells for 24 h along with control group.

Panel A: Images were obtained using an inverted Phase contrast microscope (Figure 7a).

Panel B: The cells were stained using AO/EtBr, and the images were obtained using an inverted Fluorescent microscope. Scale Bar (100 μm). The histogram represents the % of Apoptotic cells in TF and LP treated groups compared with control groups on MDA-MB-231 cells (Figure 7b).

Cells were treated with TF and LP (20 and 30 $\mu\text{g/ml}$) on MDA-MB-231 cells for 24 h along with control group.

Panel A: The cells were stained using DCFH-DA dye, and the images were obtained using an inverted fluorescent microscope. Scale Bar (100 μm). The histogram represents the % relative fluorescence in TF and LP treated groups compared with control groups on MDA-MB-231 cells (Figure 7c).

Panel B: The cells were stained using DAPI, and the images were obtained using an inverted fluorescent microscope. Scale Bar (100 μm). The histogram represents the number of (%) Apoptotic cells in TF and LP treated groups compared with control groups on MDA-MB-231 cells (Figure 7d).

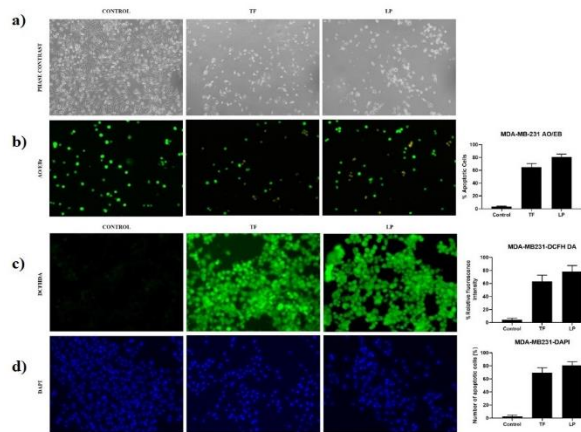


Figure 7. a) phase contrast images of MDA-MB-231 cells on treatment with control, Tipifarnib (TF), Liposomal Tecomaquinone I (LP) b) shows inverted fluorescent microscopy images of the MDA-MB-231 cells and the graph shows the % of apoptotic cells c) shows DCFH/DA dye stained MDA-MB-231 cells and the graph shows the % of relative fluorescence intensity d) shows DAPI stained MDA-MB-231 cells and the graph shows the number of apoptotic cells

TF and LP (20 and 30 µg/ml) on A549

Cells were treated with TF and LP (20 and 30 µg/ml) on A549 cells for 24 h along with control group.

Panel A: Images were obtained using an inverted Phase contrast microscope (Figure 8a).

Panel B: The cells were stained using AO/EtBr, and the images were obtained using an inverted fluorescent microscope. Scale Bar (100µm)

The histogram represents the % of Apoptotic cells in TF and LP treated groups compared with control groups on A549 cells (Figure 8b).

Cells were treated with TF and LP (20 and 30 µg/ml) on A549 cells for 24 h along with control group.

Panel A: The cells were stained using DCFH-DA dye, and the images were obtained using an inverted fluorescent microscope. Scale Bar (100µm), The histogram represents the % relative fluorescence in TF and LP treated groups compared with control groups on A549 cells (Figure 8c).

Panel B: The cells were stained using DAPI, and the images were obtained using an inverted fluorescent microscope. Scale Bar (100µm), The histogram represents the number of (%) Apoptotic cells in TF and LP treated groups compared with control groups on A549 cells (Figure 8d).

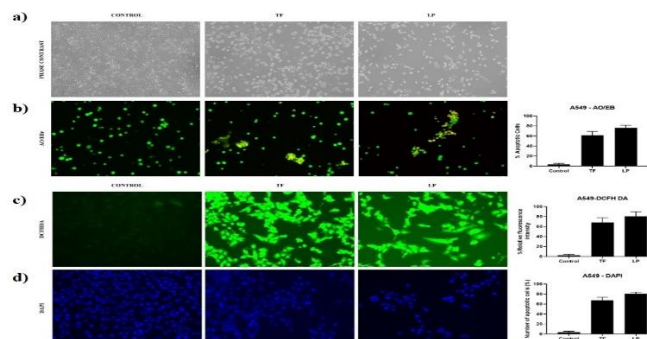


Figure 8. a) phase contrast images of A549 cells on treatment with control, Tipifarnib (TF), Liposomal Tecomaquinone I (LP) b) shows inverted fluorescent microscopy images of the A549 cells and the graph shows the % of apoptotic cells c) shows DCFH/DA dye stained A549 cells and the graph shows the % of relative fluorescence intensity d) shows DAPI stained A549 cells and the graph shows the number of apoptotic cells

TF and LP (20 and 30 µg/ml) on SCC-25 cells:

Cells were treated with TF and LP (20 and 30 µg/ml) on SCC-25 cells for 24 h along with control group.

Panel A: Images were obtained using an inverted Phase contrast microscope (Figure 9a).

Panel B: The cells were stained using AO/EtBr, and the images were obtained using an inverted fluorescent microscope. Scale Bar (100µm)

The histogram represents the % of Apoptotic cells in TF and LP treated groups compared with control groups on SCC-25 cells (Figure 9b).

Cells were treated with TF and LP (20 and 30 µg/ml) on SCC-25 cells for 24 h along with control group.

Panel A: The cells were stained using DCFH-DA dye, and the images were obtained using an inverted fluorescent microscope. Scale Bar (100µm), The histogram represents the % relative fluorescence in TF and LP treated groups compared with control groups on SCC-25 cells (Figure 9c).

Panel B: The cells were stained using DAPI, and the images were obtained using an inverted fluorescent microscope. Scale Bar (100µm), The histogram represents the number of (%) Apoptotic cells in TF and LP treated groups compared with control groups on SCC-25 cells (Figure 9d).

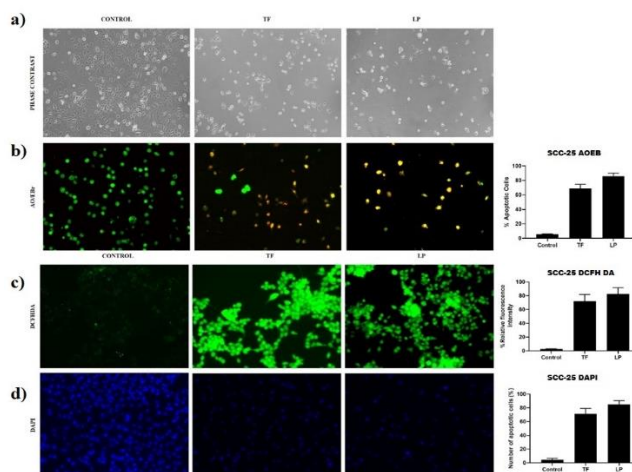


Figure 9. a) phase contrast images of SCC-25 cells on treatment with control, Tipifarnib (TF), Liposomal Tecomaquinone I (LP) b) shows inverted fluorescent microscopy images of the SCC-25 cells and the graph shows the % of apoptotic cells c) shows DCFH/DA dye stained SCC-25 cells and the graph shows the % of relative fluorescence intensity d) shows DAPI stained SCC-25 cells and the graph shows the number of apoptotic cells

Cell Cycle Analysis

TF and LP (20 & 30 µg/ml) on MDA-MB-231 Cells

Measurement of cell cycle populations after treatment with TF and LP (20 & 30 µg/ml) on MDA-MB-231 cells for 24 h along with control group.

The Cell cycle analysis are done using a DNA intercalating dye, such as PI, to quantify the amount of DNA present in each cell. The

histogram shows the percentage of cell cycle progression in MDA-MB-231 cancer cells treated with TF& LP and untreated control cells for 24hrs (Figure 10a).

This FACS data demonstrates the effects of TF and LP treatments on apoptosis and cell cycle progression in MDA-MB-231 cells. Annexin V/PI staining shows that control cells remain primarily viable (lower-left quadrant), while TF treatment leads to a increase in apoptotic cells (upper-right and lower-right

quadrants). LP treatment induces a higher level of apoptosis compared to control, but slightly lesser than TF, as evidenced by the significant population shift to the upper-right quadrant. In terms of cell cycle dynamics, propidium iodide staining reveals that control cells are mainly in the G0/G1 phase. TF treatment results in an increase in the S-phase population, indicating replication stress. LP treatment, on the other hand, causes a marked accumulation of cells in the G2/M phase, suggesting mitotic arrest. The accompanying bar graph confirms these observations, showing a decrease in the G0/G1 phase and an increase in S and G2/M phases with TF and LP, respectively. Overall, LP is more effective than TF in inducing apoptosis and disrupting the cell cycle, with its primary impact being G2/M arrest and enhanced cell death.

TF and LP (20 & 30 µg/ml) on A549 Cells

Measurement of cell cycle populations after treatment with TF and LP (20 & 30 µg/ml) on A549 cells for 24 h along with a control group. The Cell cycle analysis are done using a DNA intercalating dye, such as PI, to quantify the amount of DNA present in each cell. The histogram shows the percentage of cell cycle progression in A549 cancer cells treated with TF& LP and untreated control cells for 24hrs (Figure 10b).

The FACS data shows the effects of TF and LP treatments on apoptosis and the cell cycle in A549 cells. Annexin V/PI staining reveals a shift from live cells (lower-left quadrant) in the control to significant apoptosis with TF (upper-right and lower-right quadrants) and an even greater apoptotic response with LP. Quantitatively, LP induces the highest levels of late apoptosis/necrosis compared to TF. Cell cycle analysis using propidium iodide indicates that control cells are predominantly in the G0/G1 phase, while TF treatment causes an increase in the S-phase population, suggesting replication stress. In contrast, LP treatment results in a pronounced accumulation of cells in

the G2/M phase, indicative of mitotic arrest. The bar graph highlights these changes, with LP showing the greatest disruption to cell cycle progression and the strongest apoptotic effect. Overall, LP appears more effective than TF in both inducing apoptosis and altering cell cycle dynamics, with its primary impact being G2/M arrest and enhanced cell death.

TF and LP (20 & 30 µg/ml) on SCC-25 Cells

Measurement of cell cycle populations after treatment with TF and LP (20 & 30 µg/ml) on SCC-25 cells for 24 h along with a control group. The Cell cycle analysis are done using a DNA intercalating dye, such as PI, to quantify the amount of DNA present in each cell. The histogram shows the percentage of cell cycle progression in SCC-25 cancer cells treated with TF& LP and untreated control cells for 24hrs (Figure 10c).

This FACS data highlights the effects of TF and LP treatments on apoptosis and cell cycle dynamics in SCC-25 cells. Annexin V/PI staining reveals that control cells predominantly remain viable (lower-left quadrant). With TF treatment, there is a significant increase in apoptosis, reflected in the higher cell populations in the upper-right (late apoptotic/necrotic) and lower-right (early apoptotic) quadrants. LP treatment further enhances this apoptotic response, with the most pronounced shift toward the upper-right quadrant. Cell cycle analysis through propidium iodide staining shows that control cells are primarily in the G0/G1 phase. TF treatment induces an increase in the S-phase population, suggesting a disruption in DNA replication. LP treatment, however, leads to a substantial accumulation of cells in the G2/M phase, indicative of mitotic arrest. The bar graph supports these findings, showing a decrease in the G0/G1 phase and increased percentages in the S and G2/M phases with TF and LP treatments, respectively. Overall, LP treatment is more potent than TF in both inducing apoptosis and causing cell cycle

disruption, with its major effect being G2/M phase arrest and enhanced apoptotic cell death.

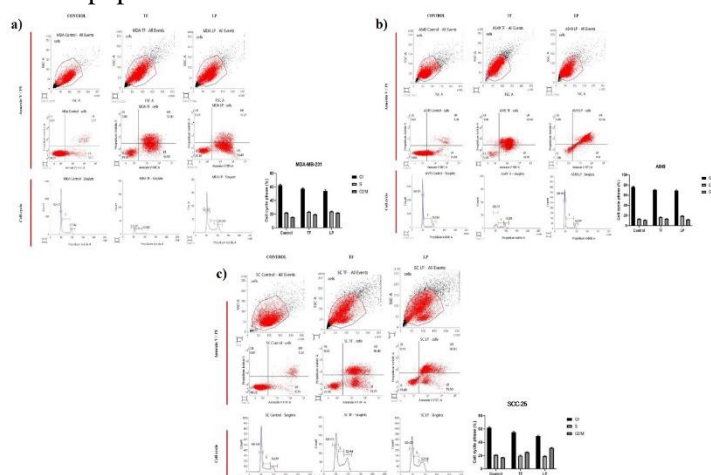


Figure 10. a) the cell cycle analysis of MDA-MB-231 after the treatment with control, Tipifarnib (TF), Liposomal tecomaquinone I (LP), b) the cell cycle analysis of A549 after the treatment with control, Tipifarnib (TF), Liposomal tecomaquinone I (LP), c) the cell cycle analysis of SCC-25 after the treatment with control, Tipifarnib (TF), Liposomal tecomaquinone I (LP).

Discussion

Phytochemicals have been proven to be an alternative chemotherapeutic agent due to their high anti-cancer potential. However, the effect of Tecomaquinone I in oral squamous cell carcinoma remains unexplored. Therefore, the purpose of the present study was to investigate the cytotoxic and apoptotic effects of the liposomal drug delivery of Tecomaquinone I in oral squamous cell carcinoma cell line. Cancer is one of the leading causes of morbidity and mortality in the world. A global cancer survey by WHO in 2018 reported 18.1 million new cancer cases and 9.6 million deaths [32]. The incidence and mortality are expected to rise to 29.5 million and 16.3 million by the year 2040 increasing the cancer burden. In the year 2022, around 1,45,844 new male oral cancer cases and 52,594 new female oral cancer cases were reported [33]. HRAS protein regulates the cell proliferation, differentiation and survival by the process of farnesylation. Farnesyl transferase plays a crucial role in the attachment of farnesyl lipid group to the signal transduction proteins which drives the progression of the cell cycle during farnesylation [34]. Farnesyl transferase inhibitor plays a vital role in the inhibition of

farnesylation prohibiting the cellular differentiation, proliferation and survival. In our study, we have used a phytochemical named Tecomaquinone I as a natural farnesyl transferase inhibitor. The treatment of OSCC cell line (SCC-25) with Tecomaquinone I showed that a substantial accumulation of cells in the G2/M phase, indicative of mitotic arrest and enhanced apoptotic cell death. It is seen that the Tecomaquinone I is more effective than Tipifarnib in inducing apoptosis and cell cycle disruption in SCC-25. We also treated MDA MB 231 A549 cells with Tecomaquinone I that showed highest level of late apoptosis/ necrosis.

Conclusion

Tecomaquinone I is a natural farnesyl transferase inhibitor and has the potential to be a safer chemotherapeutic agent. It has better cytotoxic and inhibitory effects on cell proliferation by inducing apoptosis in oral squamous cell carcinoma. Further in vivo studies should be conducted to prove the anti-cancer effect of Tecomaquinone I in oral squamous cell carcinoma.

Conflict of Interest

The authors declare that there is no conflict of interest.

References

- [1]. Tiwari, G., Tiwari, R., Bannerjee, S., Bhati, L., Pandey, S., Pandey, P., Sriwastawa, B., 2012, Drug delivery systems: An updated review. *International Journal of Pharmaceutical Investigation*, 2:2.
- [2]. Nsairat, H., Khater, D., Sayed, U., Odeh, F., Bawab, A. A., Alshaer, W., 2022, Liposomes: structure, composition, types, and clinical applications. *Heliyon*, 8:e09394.
- [3]. Jha, S., Sharma, P. K., Malviya, R., 2016, Liposomal Drug delivery system for cancer therapy: advancement and patents. *Recent Patents on Drug Delivery & Formulation*, 10, 177–183.
- [4]. Cabanes, A., Even-Chen, S., Zimberoff, J., Barenholz, Y., Kedar, E., Gabizon, A., 1999, Enhancement of antitumor activity of polyethylene glycol-coated liposomal doxorubicin with soluble and liposomal interleukin 2. *Clin Cancer Res*, 5, 687–93.
- [5]. Fassas, A., Anagnostopoulos, A., 2005, The use of liposomal daunorubicin (DaunoXome) in acute myeloid leukemia. *Leukemia & Lymphoma/Leukemia and Lymphoma*, 46, 795–802.
- [6]. Rudramurthy, S. M., Jatana, M., Singh, R., Chakrabarti, A., 2012, In vitro antifungal activity of Indian liposomal amphotericin B against clinical isolates of emerging species of yeast and moulds, and its comparison with amphotericin B deoxycholate, voriconazole, itraconazole and fluconazole. *Mycoses*, 56, 39–46.
- [7]. Chang, H. I., Yeh, M. K., 2011, Clinical development of liposome based drugs: formulation, characterization, and therapeutic efficacy. *International Journal of Nanomedicine*, 49–60.
- [8]. Angst, M. S., Drover, D. R., 2006, Pharmacology of Drugs Formulated with DepoFoam???. *Clinical Pharmacokinetics*, 45, 1153–1176.

Acknowledgements

We would like to acknowledge the Madurai Kamaraj University, for their unwavering support in material analysis.

- [9]. Ghantous, Y., Elnaaj, A. I., 2017, Global Incidence and Risk Factors of Oral Cancer. *Harefuah*, 156, 645–649.
- [10]. Nethan, S. T., Ravi, P., Gupta, P. C., 2022, Epidemiology of Oral Squamous Cell Carcinoma in Indian Scenario. In: Routray, S., (eds) *Microbes and Oral Squamous Cell Carcinoma*, Springer, Singapore, pp 1–7
- [11]. Mehrotra, R., Yadav, S., 2006, Oral squamous cell carcinoma: Etiology, pathogenesis and prognostic value of genomic alterations. *Indian Journal of Cancer*, 43(2), 60-6.
- [12]. Reichal, P., Ramani, P., Kizhakkootu, S., 2024, Association of site and recurrence in oral squamous cell carcinoma patients visiting private hospital in Chennai: a retrospective study. *Cureus*, 16(1), e52774. <https://doi.org/10.7759/cureus.52774>
- [13]. Thomas, P., Mathew, D., Anisha, K., Ramasubramanian, A., Ramalingam, K., Ramani, P., Sekar, D., 2024, A retrospective analysis of the clinicopathological profile of oral squamous cell carcinoma in tobacco and non-tobacco users: highlighting the significance of chronic mechanical irritation. *Cureus*, 16(5), e59953. <https://doi.org/10.7759/cureus.59953>.
- [14]. Pérez-Sayáns, N., 2009, Genetic and molecular alterations associated with oral squamous cell cancer (Review). *Oncology Reports*, 22(6), 1277-82. https://doi.org/10.3892/or_00000565.
- [15]. Field, J. K., 1995, The role of oncogenes and tumour-suppressor genes in the aetiology of oral, head and neck squamous cell carcinoma. *J R Soc Med*, 88(1), 35P-39P.
- [16]. Murugan, A. K., Munirajan, A. K., Tsuchida, N., 2012, Ras oncogenes in oral cancer: The past 20 years. *Oral Oncology*, 48(5), 383–392.
- [17]. Devi, P., Dwivedi, R., Sankar, R., Jain, A., Gupta, S., Gupta S., 2024, Unraveling the Genetic Web: H-Ras Expression and Mutation in Oral

- Squamous Cell Carcinoma—A Systematic Review. *Head and Neck Pathology*, 18(1), 21. <https://doi.org/10.1007/s12105-024-01623-8>.
- [18]. Palsuledesai, C. C., Distefano, M. D., 2015, Protein prenylation: enzymes, therapeutics, and biotechnology applications. *ACS Chemical Biology*, 10(1), 51–62.
- [19]. Simanshu, D. K., Nissley, D. V., McCormick, F., 2017, RAS proteins and their regulators in human disease. *Cell*, 170(1), 17–33.
- [20]. Rowinsky, E. K., Windle, J. J., Von Hoff, D. D., 1999, RAS protein farnesyltransferase: a strategic target for anticancer therapeutic development. *Journal of Clinical Oncology*, 17(11), 3631–3652.
- [21]. Umashankar, K., Selvaraj, J., Ramani, P., 2021, Expression of ITG β -1, MMP9 and Vimentin in Oral Squamous Cell Carcinoma – A Real Time PCR Based Approach. *Journal of Pharmaceutical Research International*, 33(44B), 81–87.
- [22]. Oladeji, O., 2016, The characteristics and roles of medicinal plants: Some important medicinal plants in Nigeria. *Natural Products: An Indian Journal*, 12(3), 102.
- [23]. Desai, A., Qazi, G., Ganju, R., El-Tamer, M., Singh, J., Saxena, A., Bedi, Y., Taneja, S., Bhat, H., 2008, Medicinal plants and cancer chemoprevention. *Current Drug Metabolism*, 9(7), 581–591.
- [24]. Greenwell, M., Rahman, P., 2015, Medicinal plants: their use in anticancer treatment. *International Journal of Pharmaceutical Sciences and Research*, 6(10), 4103-4112. [https://doi.org/10.13040/ijpsr.0975-8232.6\(10\).4103-12](https://doi.org/10.13040/ijpsr.0975-8232.6(10).4103-12).
- [25]. Goswami, D., Nirmal, S., Patil, M., Dighe, N., Laware, R., Pattan, S., 2009, An overview of *Tectona grandis*: chemistry and pharmacological profile. *Pharmacognosy Reviews*, 3(5), 181–185.
- [26]. Cadelis, M. M., Bourguet-Kondracki, M. L., Dubois, J., Valentin, A., Barker, D., Copp, B. R., 2016, Discovery and preliminary structure–activity relationship studies on Tecomaquinone I and tectol as novel farnesyltransferase and plasmodial inhibitors. *Bioorganic & Medicinal Chemistry*, 22(14), 3102–3107.
- [27]. Rafique, M., Sadaf, I., Rafique, M. S., Tahir, M. B., 2016, A review on green synthesis of silver nanoparticles and their applications. *Artificial Cells, Nanomedicine and Biotechnology*, 45(7), 1272–1291.
- [28]. Kavitha, R. K., Vijayalakshmi, S., Babu M. B., 2019, Synthesis and Characterization of Silver Nano Particles using Tecoma Stans Flower Extract. *International Journal of Recent Technology and Engineering (IJRTE)*, 8(4), 5624–5629.
- [29]. Lombardo, D., Kiselev, M. A., 2022, Methods of liposomes preparation: Formation and control factors of versatile nanocarriers for biomedical and nanomedicine application. *Pharmaceutics*, 14(3), 543.
- [30]. Lu, W. L., Qi X. R., 2017, Liposome-Based drug delivery systems. *Biomaterial engineering*, <https://doi.org/10.1007/978-3-662-49231-4>.
- [31]. Lasch, J., Weissig, V., Brandl, M., 2003, Preparation of liposomes. In: *Liposomes - A Practical Approach*. 2nd edition. Oxford University Press eBooks, pp 1–29.
- [32]. Bray, F., Ferlay, J., Soerjomataram, I., Siegel, R. L., Torre, L. A., Jemal, A., 2018, Global cancer statistics 2018: GLOBOCAN estimates of incidence and mortality worldwide for 36 cancers in 185 countries. *CA Cancer J Clin*, 68(6), 394–424.
- [33]. Mathur, P., Sathishkumar, K., Chaturvedi, M., Das, P., Stephen, S., 2022, Cancer incidence estimates for 2022 & projection for 2025: Result from National Cancer Registry Programme, India. *Indian J Med Res*, 156(4&5), 598-607.
- [34]. Long, S. B., Casey, P. J., Beese, L. S., 2002, Reaction path of protein farnesyltransferase at atomic resolution. *Nature*, 419(6907), 645–650.